Available online at www.sciencedirect.com
SCIENCE DIRECT®
Journal of Computational Physics 191 (2003) 639–659
JOURNAL OF COMPUTATIONAL PHYSICS
www.elsevier.com/locate/jcp

A weighted essentially non-oscillatory numerical scheme for a multi-class Lighthill–Whitham–Richards traffic flow model

Mengping Zhang [a], Chi-Wang Shu [b,*], George C.K. Wong [c], S.C. Wong [c]

[a] Department of Mathematics, University of Science and Technology of China, Hefei, Anhui 230026, PR China
[b] Division of Applied Mathematics, Brown University, Providence, RI 02912, USA
[c] Department of Civil Engineering, The University of Hong Kong, Pokfulam Road, Hong Kong, PR China

Received 17 March 2003; received in revised form 16 June 2003; accepted 24 June 2003

Abstract

In this paper, we present a high-order weighted essentially non-oscillatory (WENO) scheme for solving a multi-class extension of the Lighthill–Whitham–Richards (LWR) model. We first review the multi-class LWR model and present some of its analytical properties. We then present the WENO schemes, which were originally designed for computational fluid dynamics problems and for solving hyperbolic conservation laws in general, and demonstrate how to apply these to the present model. We found through numerical experiments that the WENO method is vastly more efficient than the low-order Lax–Friedrichs scheme, yet both methods converge to the same solution of the physical model. It is especially interesting to observe the small staircases in the solution which are completely missed out, because of the numerical viscosity, if a lower-order method is used without a sufficiently refined mesh. To demonstrate the applicability of this new, efficient numerical tool, we study the multi-class model under different parameter regimes and traffic stream models. We consider also the convergence of the multi-class LWR model when the number of classes goes to infinity. We show that the solution converges to a smooth profile without staircases when the number of classes increases.

AMS: 65M06; 90B20

Keywords: Multi-class LWR model; Traffic flow; Weighted essentially non-oscillatory scheme; Lax–Friedrichs scheme; Godunov scheme

1. Introduction

Lighthill and Whitham [21] and Richards [24] independently proposed a simple continuum model, now known as the LWR model, to describe the characteristics of traffic flow. In this model, a traffic stream model (a relationship between the traffic state variables of flow, speed and density, e.g. [13]) is supplemented by the

* Corresponding author. Tel.: +1-401-863-2549; fax: +1-401-863-1355.
E-mail address: shu@dam.brown.edu (C.-W. Shu).

0021-9991/$ - see front matter © 2003 Elsevier B.V. All rights reserved.
doi:10.1016/S0021-9991(03)00344-9

continuity equation of vehicles, and the resultant partial differential equation presumably could be solved to obtain the density as a function of space and time. For a specific form of Greenshields' traffic stream model, the solution can be obtained analytically [31]. Although aiming to provide a coarse representation of traffic behavior, the LWR model is capable of reproducing qualitatively a remarkable amount of real traffic phenomena, such as shock formation. Nevertheless, there are still some puzzling traffic phenomena observed on the highway, such as the two-capacity or reverse-λ state in the fundamental diagram, hysteresis of traffic flow and platoon dispersion, that this simple LWR model cannot address or explain.

Recently, multi-class models have been developed in an attempt to explain these puzzling traffic phenomena by modeling users' lane changing behavior and/or multiple vehicle types [1,6–9,14–16,32,33]. Wong and Wong [30] formulated a multi-class model with heterogeneous drivers (MCLWR model), which was extended from the LWR model. Although the MCLWR model is simple in nature, it was found that the model is capable of producing the desired properties of a macroscopic traffic flow model and it explains many puzzling phenomena, such as the two-capacity or reverse-λ state, hysteresis and platoon dispersion, but it would not be subject to other deficiencies such as wrong-way travel [5].

In [30], the MCLWR model was solved by a first-order Lax–Friedrichs finite difference scheme. Although this finite difference scheme is commonly used to solve the original LWR model [18,23], it is argued that this first-order Lax–Friedrichs scheme may produce smeared solutions near discontinuities due to excessive numerical viscosity. The effect of numerical viscosity will diminish with mesh refinement, but it will be very costly to solve a very refined mesh. More recently, Lebacque [19] successfully applied the Godunov scheme, introduced by Godunov [11], to solve the LWR model. The Godunov scheme is subject to smaller numerical viscosity, but it requires a Riemann solver as its building block, which is very difficult, if not impossible, to develop for the MCLWR model. This is because the multi-class model does not seem to be either genuinely nonlinear or linearly degenerate [20]. Nevertheless, it is important to note that, even though for first-order methods the Godunov scheme is more accurate than the Lax–Friedrichs scheme, this difference diminishes dramatically when higher-order schemes are considered [25]. Both Godunov and Lax–Friedrichs schemes converge to the same physical solution of the model with a sufficiently refined mesh. This can be proved for the scalar and some system cases, and can be observed for more complex systems [20,25].

This paper presents the solution of the MCLWR model by a weighted essentially non-oscillatory (WENO) scheme [17]. The WENO scheme is a very robust numerical scheme and is found to be very useful in computational fluid dynamics as well as in other applications. The numerical results from WENO are compared with those obtained from the first-order Lax–Friedrichs method. In the special case, when all the eigenvalues of the kinematic wave matrix of the system (6) are positive, the Godunov solver becomes the simple upwind solver. In this special case, we have verified that the first-order Godunov solver converges faster than the first-order Lax–Friedrichs solver, but slower than the fifth-order WENO solver, while all three converge to the same physical solution. In Section 2, the MCLWR model is introduced. The WENO scheme for the MCLWR is given in Section 3. Section 4 compares the convergence characteristics of the numerical schemes, shows the numerical solutions for different congestion regimes, and studies the asymptotic case of an infinite number of classes.

2. The MCLWR model

2.1. The model

Let there be M classes of road users with different speed choice behaviors in response to the same traffic density when traveling on a highway section. It means that for a given total density, there exists a distribution of equilibrium speeds by different user classes. It is expected that the variation around the mean speed (averaged over all user classes) decreases when traffic density increases, due to the tighter interactions

between road users. Let $q_m(x,t), k_m(x,t)$ and $u_m(x,t)$ be, respectively, the flow, density and speed of user class m in the space–time domain. The total density on a highway section can then be obtained as

$$k(x,t) = \sum_{m=1}^{M} k_m(x,t). \tag{1}$$

The flow, density and speed variables of a particular class are subject to the following definitional relationship:

$$q_m(x,t) = u_m(x,t) \cdot k_m(x,t) \quad \forall m = 1,2,\ldots,M. \tag{2}$$

From the law of conservation of vehicles, each user class should satisfy the following continuity equation:

$$\frac{\partial k_m(x,t)}{\partial t} + \frac{\partial q_m(x,t)}{\partial x} = 0 \quad \forall m = 1,2,\ldots,M, \tag{3}$$

which describes the conservation of vehicles at any location at any time along a topographically homogeneous highway section without intermediate entrances or exits.

The core of the present extension is to assume that the choice of speed of a particular user class is not only affected by the presence of this user class, but also by all other user classes on the highway. A general form of speed–density relationship can be written as

$$u_m(x,t) = U_m(k_1,k_2,\ldots,k_M) \quad \forall m = 1,2,\ldots,M. \tag{4}$$

For the isotropic case, the above relationship would take a simpler functional form as

$$u_m(x,t) = U_m(k) \quad \forall m = 1,2,\ldots,M, \tag{5}$$

where k is the total density determined by Eq. (1).

Combining the above equations, the problem can be formulated into a set of partial differential equations,

$$\frac{\partial k_m(x,t)}{\partial t} + \sum_{n=1}^{M} c_{mn}(x,t)\frac{\partial k_n(x,t)}{\partial x} = 0 \quad \forall m = 1,2,\ldots,M, \tag{6}$$

where

$$c_{mn} = U_m\delta_{mn} + k_m\frac{\partial U_m}{\partial k_n} \quad \forall m,n = 1,2,\ldots,M \tag{7}$$

is the kinematic wave speed of user class m in response to the presence of class n users, and $\delta_{mn} = 1$ if $m = n$; and $\delta_{mn} = 0$ if $m \neq n$. Note that the problem stipulated in Eq. (6) reduces to the original LWR model when $M = 1$ (i.e., homogeneous users). The problem becomes one of solving the set of differential equation (6), or better still the conservation form (3) with q_m defined by Eq. (2) and u_m defined by Eq. (5), subject to certain initial spatial and time boundary conditions. The conservation form is used because when the solution becomes discontinuous (containing shocks or other discontinuities), the two systems (3) and (6) are *not* equivalent. Thus to be on the safer side, one should always use conservative scheme to solve (3) directly.

2.2. Hyperbolicity of the system

Let $\mathbf{k} = \mathrm{Col}(k_1,k_2,\ldots,k_M)$ be a column vector containing all M density variables in the MCLWR model. For a *smooth* solution $\mathbf{k}$ (meaning that $\mathbf{k}$ has at least first-order continuous derivatives in x and t), the set of partial differential equations (PDEs) (3) can be rewritten as

$$\frac{\partial \mathbf{k}}{\partial t} + \mathbf{A}(\mathbf{k})\frac{\partial \mathbf{k}}{\partial x} = 0, \tag{8}$$

where $\mathbf{A}(\mathbf{k}) = \nabla_{\mathbf{k}}\mathbf{q}(\mathbf{k})$ is a kinematic wave matrix containing all the elements of c_{mn} in Eq. (7), and $\mathbf{q} = \mathrm{Col}(q_1, q_2, \ldots, q_M)$ is a column vector of the flow fluxes of all classes. The system (3) is called hyperbolic if the eigenvalues of the kinematic wave matrix $\mathbf{A}(\mathbf{k})$ are all real and there is a complete, linearly independent set of eigenvectors. Hyperbolic systems are mathematically well-posed, meaning that their solutions depend continuously on the initial conditions. This can be proved for the linear case and also for some nonlinear cases. An important issue in verifying the reasonableness of a model is to check if it is hyperbolic. We confirm that the system (3) is hyperbolic for the practical choices of traffic stream models and their parameters. This verification is performed analytically for the two-class case and numerically for the general M-class case to be discussed in Section 4.

For the two-class case ($M = 2$), the kinematic wave matrix is a 2×2 matrix given by

$$\mathbf{A} = \begin{bmatrix} U_1(k) + k_1 U_1'(k) & k_1 U_1'(k) \\ k_2 U_2'(k) & U_2(k) + k_2 U_2'(k) \end{bmatrix}, \tag{9}$$

where $U_1(k)$ and $U_2(k)$ are defined in Eq. (5). The two eigenvalues of the kinematic wave matrix are thus given by

$$\lambda_{1,2} = (U_1(k) + k_1 U_1'(k) + U_2(k) + k_2 U_2'(k) \pm \sqrt{D})/2, \tag{10}$$

where

$$D = \big(\big(U_1(k) + k_1 U_1'(k)\big) - \big(U_2(k) + k_2 U_2'(k)\big)\big)^2 + 4k_1 k_2 U_1'(k) U_2'(k). \tag{11}$$

Clearly $D > 0$ which implies that the two eigenvalues are both real and distinct. Thus the system is hyperbolic.

We could obtain analytical formulas for the eigenvalues of the kinematic wave matrix for the three-class or even the four-class case ($M = 3$ or 4), however, the formulas are quite complex and it is not easy to see whether the eigenvalues are always real. At any rate, this approach would not work for the multi-class case with $M > 4$, as no analytical formulas for the eigenvalues would be available. This is a disadvantage when compared with some other multi-class models [1,6–9,14–16,32,33], as our system is large and its hyperbolicity cannot be easily proven. However, this problem can be overcome as hyperbolicity can be checked numerically.

We thus resort to implementing a numerical eigenvalue solver to verify a posteriori that the eigenvalues are always real for all the test cases in [30] and in this paper. Indeed through all the numerical tests, non-real eigenvalues never appear for the kinematic wave matrix. Although this is not a rigorous proof that the MCLWR model is always hyperbolic, it at least gives validity to the numerical experiments in [30] and in this paper as the models under all these cases are hyperbolic.

2.3. First-order traveling waves

In this section, we apply a linearization approach to demonstrate the traveling wave properties of the MCLWR model [28]. To simplify the analysis, we also consider the simple two-class system and assume a modified Greenshields' form of traffic stream model,

$$u_1 = u_{f1}\left(1 - \frac{k_1 + k_2}{k_{\mathrm{jam}}}\right) \quad \text{and} \quad u_2 = u_{f2}\left(1 - \frac{k_1 + k_2}{k_{\mathrm{jam}}}\right), \tag{12}$$

where, for Class 1 and Class 2 traffic, u_1 and u_2 are the traffic speeds, k_1 and k_2 are the densities, and u_{f1} and u_{f2} are the free-flowing speeds, respectively, while k_{jam} is the jam density of the highway. The system of differential equations can be written as

$$\frac{\partial k_1}{\partial t}+\frac{\partial(u_1k_1)}{\partial x}=0 \quad \text{and} \quad \frac{\partial k_2}{\partial t}+\frac{\partial(u_2k_2)}{\partial x}=0. \tag{13}$$

For small perturbations of densities, r and w, around the steady-state densities $\bar{k}_1$ and $\bar{k}_2$, respectively, we can write

$$k_1=\bar{k}_1+r \quad \text{and} \quad k_2=\bar{k}_2+w. \tag{14}$$

Substituting Eq. (14) into Eq. (13) and neglecting higher-order terms, we can show that

$$\frac{\partial r}{\partial t}+\frac{u_{f1}}{k_{\text{jam}}}(k_{\text{jam}}-2\bar{k}_1-\bar{k}_2)\frac{\partial r}{\partial x}=\frac{u_{f1}\bar{k}_1}{k_{\text{jam}}}\frac{\partial w}{\partial x} \tag{15}$$

and

$$\frac{\partial w}{\partial t}+\frac{u_{f2}}{k_{\text{jam}}}(k_{\text{jam}}-2\bar{k}_2-\bar{k}_1)\frac{\partial w}{\partial x}=\frac{u_{f2}}{k_{\text{jam}}}\bar{k}_2\frac{\partial r}{\partial x}. \tag{16}$$

Eliminating w from Eqs. (15) and (16), we have

$$\left(\frac{\partial}{\partial t}+\omega_1\frac{\partial}{\partial x}\right)\left(\frac{\partial}{\partial t}+\omega_2\frac{\partial}{\partial x}\right)r=\frac{\bar{k}_1\bar{k}_2u_{f1}u_{f2}}{k_{\text{jam}}^2}\frac{\partial^2 r}{\partial x^2}, \tag{17}$$

where

$$\omega_1=u_1-\frac{\bar{k}_1u_{f1}}{k_{\text{jam}}} \quad \text{and} \quad \omega_2=u_2-\frac{\bar{k}_2u_{f2}}{k_{\text{jam}}}. \tag{18}$$

In Eq. (18), the left-hand side is a wave operator, which indicates that there are two first-order traveling waves of speeds ω_1 and ω_2 in the traffic stream. It is interesting and important to note that these class-characterized waves always travel more slowly than the fastest vehicle in the traffic stream. This linearization approach can also be generalized to any number of classes. Also note that when substituting the modified Greenshields' form of traffic stream model (12) into Eq. (10), the eigenvalues are identical to the traveling wave speeds shown in Eq. (18) for this two-class case, when one of the steady-state densities k_1 or k_2 is equal to zero.

3. WENO numerical scheme

In recent years many high order, high resolution, numerical methods have been developed in the literature to solve a system of partial differential equations (PDEs). The main applications are in computational fluid dynamics, but there are also applications in other physical and engineering areas. In this paper, we apply the high-order finite difference scheme, weighted essentially non-oscillatory (WENO) scheme [2,17], to solve the MCLWR system (3). In particular, the fifth-order WENO scheme in [17] is used. The numerical procedure is summarized in this section. These numerical methods are found to be very useful because of their simultaneous high-order accuracy and non-oscillatory property in the presence of shocks and other discontinuities or sharp gradient regions in the solution, or, in general, for convection dominated problems. For more details of such methods, see Shu [25,26].

We now describe the computational procedure of the fifth-order WENO scheme. Spatial discretization is discussed first. We start from the simple case of a scalar equation (3), i.e., a one-class model, and assume $\partial q(k)/\partial k \geqslant 0$, i.e., the wind direction is positive. More general cases will be described later. The computational domain is discretized into a uniform mesh of J grid points:

$$x_j = j\Delta x; \quad j = 1, 2, \ldots, J, \tag{19}$$

where Δx is the uniform mesh size on the spatial axis. A smooth non-uniform mesh could also be used to concentrate grid points near certain regions to obtain better resolution. A conservative numerical approximation $k_j(t)$ to the exact solution $k(x_j, t)$ of (3) satisfies the following ordinary differential equation (ODE) system:

$$\frac{\mathrm{d}k_j(t)}{\mathrm{d}t} + \frac{1}{\Delta x}\left(\widehat{q}_{j+1/2} - \widehat{q}_{j-1/2}\right) = 0, \tag{20}$$

where $\widehat{q}_{j+1/2}$ is called the numerical flux, whose design is the key ingredient for a successful scheme. For the fifth-order WENO scheme, the numerical flux $\widehat{q}_{j+1/2}$ is defined as follows:

$$\widehat{q}_{j+1/2} = \upsilon_1 \widehat{q}^{(1)}_{j+1/2} + \upsilon_2 \widehat{q}^{(2)}_{j+1/2} + \upsilon_3 \widehat{q}^{(3)}_{j+1/2}, \tag{21}$$

where $\widehat{q}^{(p)}_{j+1/2}$ are the three third-order fluxes on three different stencils given by

$$\widehat{q}^{(1)}_{j+1/2} = \frac{1}{3}q_{j-2} - \frac{7}{6}q_{j-1} + \frac{11}{6}q_j, \tag{22a}$$

$$\widehat{q}^{(2)}_{j+1/2} = -\frac{1}{6}q_{j-1} + \frac{5}{6}q_j + \frac{1}{3}q_{j+1}, \tag{22b}$$

$$\widehat{q}^{(3)}_{j+1/2} = \frac{1}{3}q_j + \frac{5}{6}q_{j+1} - \frac{1}{6}q_{j+2}, \tag{22c}$$

where q_j is a short notation to denote $q(k_j(t))$, and the nonlinear weights υ_p are given by

$$\upsilon_p = \frac{\tilde{\upsilon}_p}{\sum_{l=1}^{3}\tilde{\upsilon}_l}, \quad \tilde{\upsilon}_l = \frac{\gamma_l}{(\varepsilon + \beta_l)^2}, \tag{23}$$

where ε is a parameter to prevent the denominator from becoming 0 and is fixed at $\varepsilon = 10^{-6}$ in all the computations in this paper. The choice of ε does not affect accuracy: the numerical errors can go much lower than ε, reaching machine zeros (around 10^{-13} for double precision). In Eq. (23), the linear weights γ_l are given by

$$\gamma_1 = \frac{1}{10}, \quad \gamma_2 = \frac{3}{5}, \quad \gamma_3 = \frac{3}{10} \tag{24}$$

and the smoothness indicators β_l given by

$$\beta_1 = \frac{13}{12}(q_{j-2} - 2q_{j-1} + q_j)^2 + \frac{1}{4}(q_{j-2} - 4q_{j-1} + 3q_j)^2, \tag{25}$$

$$\beta_2 = \frac{13}{12}(q_{j-1} - 2q_j + q_{j+1})^2 + \frac{1}{4}(q_{j-1} - q_{j+1})^2, \tag{26}$$

$$\beta_3 = \frac{13}{12}(q_j - 2q_{j+1} + q_{j+2})^2 + \frac{1}{4}(3q_j - 4q_{j+1} + q_{j+2})^2. \tag{27}$$

We remark that the stencil for the scheme is biased to the left because of the positive wind direction. This finishes the description of the fifth-order finite difference WENO scheme [17] for the scalar equation with a positive wind direction. As we can see, the algorithm is actually quite straightforward and there are no parameters to be tuned in the scheme. The main reason that it works well, both for smooth solutions and for solutions containing shocks or other discontinuities or high gradient regions, is that the nonlinear weights, determined by the smoothness indicators, are automatically adjusting themselves, based on the numerical solution, to use the locally smoothest information given by the solution. We refer to [2,17,25,26] for accuracy tests and computational fluid dynamics simulations using this method.

If the "wind direction" $\partial q(k)/\partial k \leqslant 0$, the procedure for computing the numerical flux $\widehat{q}_{j+1/2}$ is a mirror image with respect to the point $x_{j+1/2}$, of what is described above. The stencil would then be biased to the right. If $\partial q(k)/\partial k$ changes sign, we will use smooth flux splitting

$$q(k) = q^+(k) + q^-(k), \tag{28}$$

where $\partial q^+(k)/\partial k \geqslant 0$ and $\partial q^-(k)/\partial k \leqslant 0$, and apply the above procedures separately on each one of them. There are many choices of such flux splitting, however the most popular one is the Lax–Friedrichs flux splitting where

$$q^{\pm}(k) = \frac{1}{2}(q(k) \pm \alpha k), \tag{29}$$

with $\alpha = \max_k |\partial q(k)/\partial k|$.

For hyperbolic systems of conservation laws (3), the eigenvalues of $\mathbf{A}(\mathbf{k})$ are all real:

$$\lambda_1(k) \leqslant \cdots \leqslant \lambda_M(k). \tag{30}$$

A safe but rather expensive way to generalize scalar schemes to such system cases is to utilize local characteristic decompositions, see [25] for details. However, such a procedure depends on the explicit formulas for the eigenvectors of $\mathbf{A}(\mathbf{k})$, which are not easy to obtain for the MCLWR model when $M \geqslant 3$. We have thus adopted a simpler, component-wise generalization, namely using the Lax–Friedrichs flux splitting (29) for each equation in the system, with a common α. Ideally, α should be chosen as the largest (absolute value) eigenvalue in (30), however closed form formulas for the eigenvalues (30) are also difficult to obtain for the MCLWR model when $M \geqslant 3$. We have thus chosen α as

$$\alpha = \max(|u_1|, \ldots, |u_m|), \tag{31}$$

where the speeds u_m are defined in Eq. (5). Numerical experiments in the following section indicate that this works well for the MCLWR model.

For the time discretization, the computational domain is discretized into a mesh of N grid points: $t^{[n]} = t^{[n-1]} + \Delta t^{[n]};\ n = 1, 2, \ldots, N$, where $\Delta t^{[n]}$ is the mesh size on the time axis. We adopt the third-order TVD Runge–Kutta method [27]:

$$k^{(1)} = k^{[n]} + \Delta t^{[n]} L(k^{[n]}, t^{[n]}), \tag{32a}$$

$$k^{(2)} = \frac{3}{4}k^{[n]} + \frac{1}{4}k^{(1)} + \frac{1}{4}\Delta t^{[n]} L(k^{(1)}, t^{[n]} + \Delta t^{[n]}), \tag{32b}$$

$$k^{[n+1]} = \frac{1}{3}k^{[n]} + \frac{2}{3}k^{(2)} + \frac{2}{3}\Delta t^{[n]} L\left(k^{(2)}, t^{[n]} + \frac{1}{2}\Delta t^{[n]}\right), \tag{32c}$$

where L is the approximation to the spatial derivatives:

$$L(k,t) = -\frac{1}{\Delta x}\left(\widehat{q}_{j+1/2} - \widehat{q}_{j-1/2}\right) \approx -\frac{\partial q(k)}{\partial x} \tag{33}$$

established by the WENO procedure outlined above. This time discretization is proved stable if the first-order Euler forward time stepping of the spatial operator is stable [12,27]. Note that this time discretization is very simple and consists of convex combinations of three first-order Euler forward steps. A CFL condition is needed for stability:

$$\alpha^{[n]}\frac{\Delta t^{[n]}}{\Delta x} \leqslant \mathrm{CFL}, \tag{34}$$

where $\alpha^{[n]}$ should be taken as the largest (absolute value) eigenvalue in (30) for time level n, but for the MCLWR model it is taken as that in (31) instead. CFL should be less than one for stability and in our computation it is taken as 0.6.

4. Computational experiments

In this section, we present our computational experiments of the MCLWR model using the high-order WENO scheme, and compare the results with other numerical schemes.

4.1. Traveling wave speeds

We start with a two-class model with the modified Greenshields' form of traffic stream model as in Eq. (12). Consider a highway 2 km long with an initial platoon of maximum density 40 veh/km as shown in Fig. 1. The left boundary has no inflow (density equals 0) for all time, and the right boundary

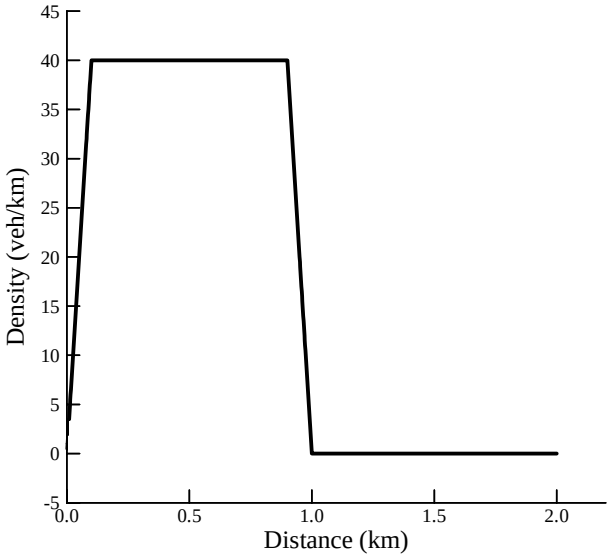

Fig. 1. Initial density platoon on the example highway.

is a free outflow (Neumann boundary condition). The free-flowing speeds of Class 1 and Class 2 drivers are 60 and 120 km/h, respectively. We assume an equal distribution of drivers in the platoon. The jam density of the highway is 200 veh/km. The dispersion of the platoon at time 0.01 h is shown in Fig. 2. It is interesting to note that the solution forms two uniform density platforms or staircases (to be discussed later) each of which contains only a single class of driver. The widths of the platforms are marked by points A, B, C and D in the figure, with the platform A–B containing Class 1 drivers only, and the platform C–D containing Class 2 drivers only. In Fig. 3, we show the speed trajectories of these points, A, B, C and D, which numerically measure the wave speeds, together with the values obtained from the eigenvalue formulas (10) and those given by the linearized formulas (18). The result shows that the linearized wave speeds give reasonable predictions of actual nonlinear wave speeds in this case.

4.2. Convergence study of the numerical methods

For a nonlinear system (3) with possible shocks and other discontinuities, it is not possible to prove mathematically that the WENO scheme, or any other scheme, converges. However, experience from computational fluid dynamics indicates that the WENO scheme is very robust and always converges for hyperbolic systems. We would like to verify through numerical experiments the convergence of the WENO scheme for the MCLWR model in this subsection.

For this purpose, we take Experiment 2 in [30] as our test case. Other test cases have also been experimented with, yielding similar results. In this experiment, we consider the same highway section and initial density platoon as that in Section 4.1, but with the number of driver classes increased to $M = 9$. The traffic stream model takes the modified Drake's form [10] as

$$u_m = U_m(k) = u_{fm} \exp(-(k/k_0)^2/2), \quad m = 1, 2, \ldots, M. \tag{35}$$

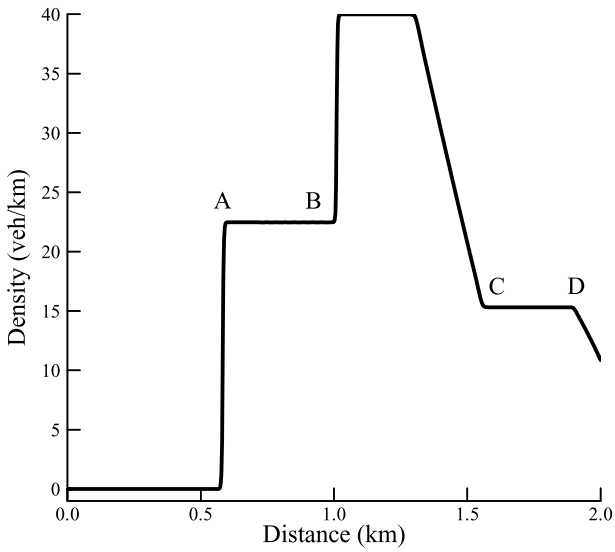

Fig. 2. The dispersion of platoon at time $t = 0.01$ h.

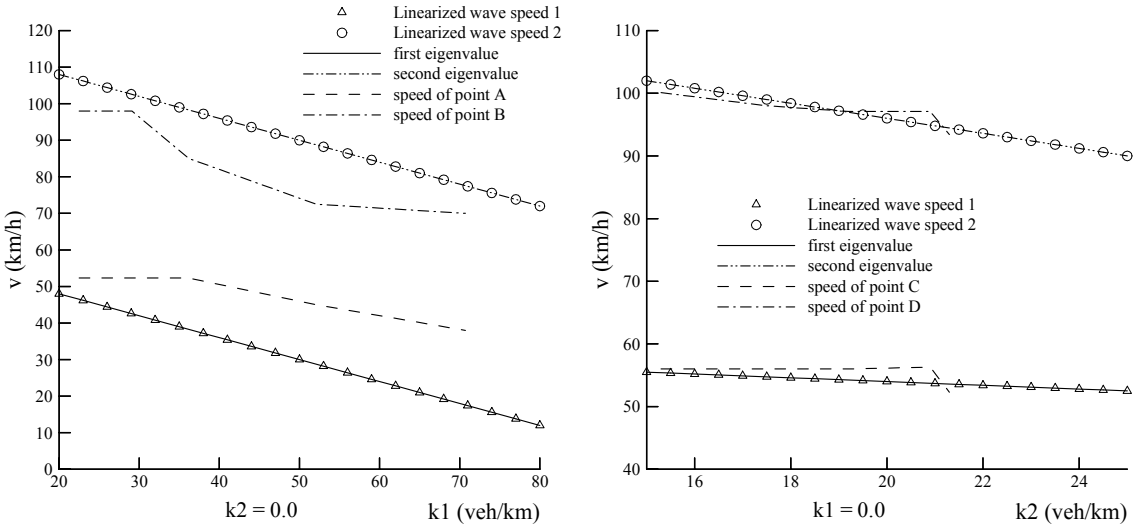

Fig. 3. The wave speeds for the two-class case.

The free flowing speeds u_{fm} of these drivers are taken as $60.0, 67.5, 75.0, \ldots, 120.0$ km/h, and the optimal density $k_0 = 50$ veh/km. The distribution in density for these user classes is given by Fig. 4. The left boundary has no inflow (density equals 0) for all time, and the right boundary is a free outflow (Neumann boundary condition). We plot the density at $t = 0.015$ h to verify numerical convergence.

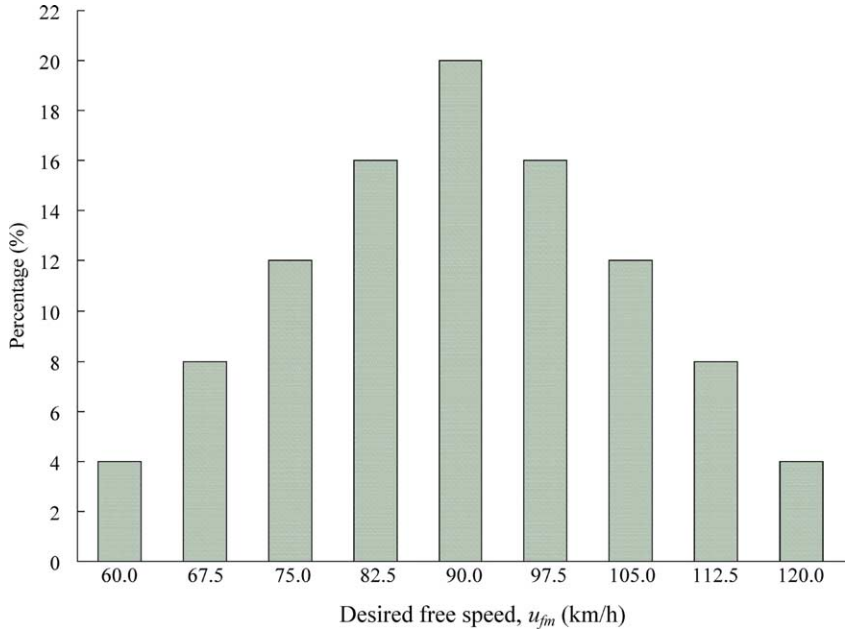

Fig. 4. Distribution of drivers in the platoon.

We first plot, in Fig. 5, top left, the total density computed with the first-order Lax–Friedrichs scheme (described in detail in [30]) using 6400 grid points (solid line), versus that computed with the fifth-order WENO scheme using 100 grid points (circles). They overlay each other quite well, indicating two things:

1. The resolution of the first-order Lax–Friedrichs scheme with 6400 points is similar to that of the fifth-order WENO scheme with 100 points. Thus the high-order WENO scheme is vastly more efficient than the first-order Lax–Friedrichs scheme for this test case.
2. If one uses only a first-order scheme to compute, one might decide prematurely that this is a convergent solution, since 6400 points make a very refined mesh.

In fact, the solution in Fig. 5, top left, is not a convergent one numerically, although the solution is good enough to demonstrate the physical characteristics of the traffic model. Nevertheless, in this paper,

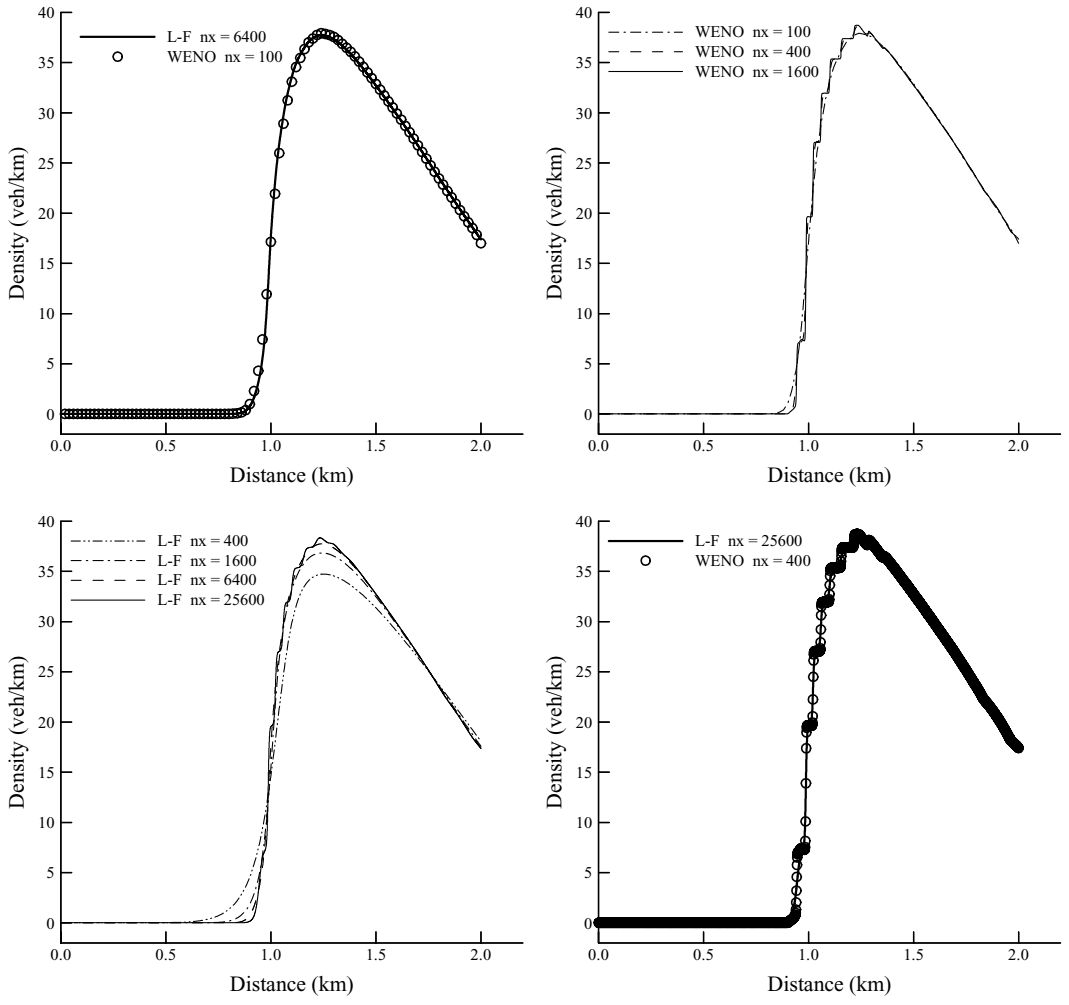

Fig. 5. Density versus distance at $t = 0.015$ h. Top left: Comparison between first-order Lax–Friedrichs with 6400 points (solid line) and WENO with 100 points (circles); Top right: Convergence of WENO with 100 points (dash-dot line), 400 points (dashed line) and 1600 points (solid line); Bottom left: Convergence of first-order Lax–Friedrichs with 400 points (dash-double dots line), 1600 points (dash-dot line), 6400 points (dashed line) and 25,600 points (solid line); Bottom right: Comparison between first-order Lax–Friedrichs with 25600 points (solid line) and WENO with 400 points (circles).

we study the numerical convergence characteristics of the traffic model in greater detail. In Fig. 5, top right, we plot the WENO solutions using 100 points (dash-dot line), 400 points (dashed line) and 1600 points (solid line). We can see that the solution has observable differences for all these grids (the difference between the 400 points and 1600 points results is small but still noticeable, especially when enlarged near the staircases). In particular, notice the small staircases in the increasing part of the solution. There are nine such small staircases, clearly related to the nine user classes. These staircases are actually shocks in different characteristic fields. The coarse mesh (100 points) WENO solution and most of the first-order Lax–Friedrichs solutions completely miss these staircases because of the excessive numerical dissipation. To verify that the numerical solution is indeed convergent, we have also computed it using WENO with 3200 grid points. The solution (not shown) completely overlays that with 1600 grid points, indicating that the WENO solution with 1600 grid points can be considered a numerically convergent solution.

In Fig. 5, bottom left, we plot the first-order Lax–Friedrichs solutions using 400 points (dash-double dot line), 1600 points (dash-dot line), 6400 points (dashed line) and 25,600 points (solid line). We can see that the solution does eventually converge with grid refinements, however, such convergence is very slow and one needs a huge number of grid points (in this case 25,600 points) to see the staircases. To convince the reader that both the WENO scheme and the Lax–Friedrichs scheme converge to the same solution, in Fig. 5, bottom right, we plot the WENO solution using 400 points (circles) and the Lax–Friedrichs solution using 25,600 points (solid line). They overlay each other quite well, both showing the small staircases.

In Fig. 6, left, we plot the total density as a function of spatial location, for various times, $t = 0, 0.005, 0.010, \ldots, 0.025$ h. We can clearly see the evolution of the dispersion of the back of the platoon and the appearance of staircases. In Fig. 6, right, we plot the flow (defined as the sum of the fluxes in (2) over all M classes) as a function of time, t, at various spatial locations, $x = 0.2, 0.4, 0.6, \ldots, 2.0$ km. We can clearly see that the small staircases are also present in these flow plots. The occurrence of these small staircases in the model results is quite consistent with the flow oscillation phenomenon that was directly observed on long homogeneous freeways [3,4,22,29]. The results in Fig. 6 are obtained using WENO with

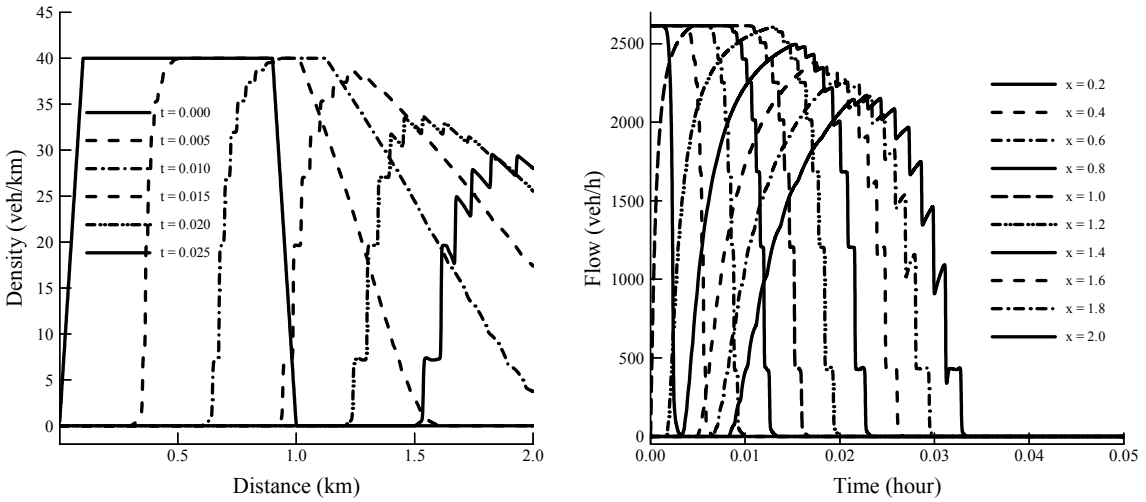

Fig. 6. Case 1. Left: total density as a function of spatial location, for $t = 0, 0.005, 0.010, \ldots, 0.025$ h; Right: the flow as a function of time t at $x = 0.2, 0.4, 0.6, \ldots, 2.0$ km.

1600 grid points, which overlays well the WENO results using 3200 grid points (not shown here), indicating that they are reliable, numerically convergent solutions of the nine-class model.

To assure the reader that these staircases are not numerical artifacts of the WENO schemes, we plot in Fig. 7 the total density as a function of spatial location, for various times, $t = 0, 0.005, 0.010, \ldots, 0.030$ h, using the nine-class model but with $u_{fm} = 90$ km/h for all nine classes. Clearly this returns to a single user model and the solution is now free from the staircases. The results in Fig. 7 are obtained using WENO schemes with 1600 grid points, which overlay the WENO results using 3200 grid points (not shown here), indicating that they are reliable, numerically convergent solutions. Note that a single user model is the original LWR model, which shows no dispersion behavior, as revealed by the figure.

In summary, in this section we have shown that

1. Using the fifth-order WENO scheme is vastly more efficient than using the first-order Lax–Friedrichs scheme, saving, by a factor of 64, on the number of mesh points needed to reach the same resolution;
2. One must be very careful in performing the grid refinement study to verify numerical convergence, for otherwise one might miss some very important solution features, such as the staircases, which might otherwise be completely obscured by numerical dissipation.
3. Both the high-order WENO scheme and the low-order Lax–Friedrichs scheme eventually converge to the same physical solution with grid refinements.

Finally in this section, we point out that we have verified a posteriori, by a numerical eigenvalue solver, that all the eigenvalues of the kinematic wave matrix stay non-negative during the time evolution. We remark that this is true only for this case and not in general for cases in the following section. For this special case, it is straightforward to write out the first-order Godunov scheme, which coincides with the simple upwind scheme (using backward difference to approximate the spatial derivatives). In Fig. 8, we show the convergence history as well as the density and flow graphs computed by the first-order Godunov scheme. We can clearly see that the resolution of the first-order Godunov scheme is better than that of the first-order Lax–Friedrichs scheme but worse than that of the fifth-order WENO scheme. Moreover, the

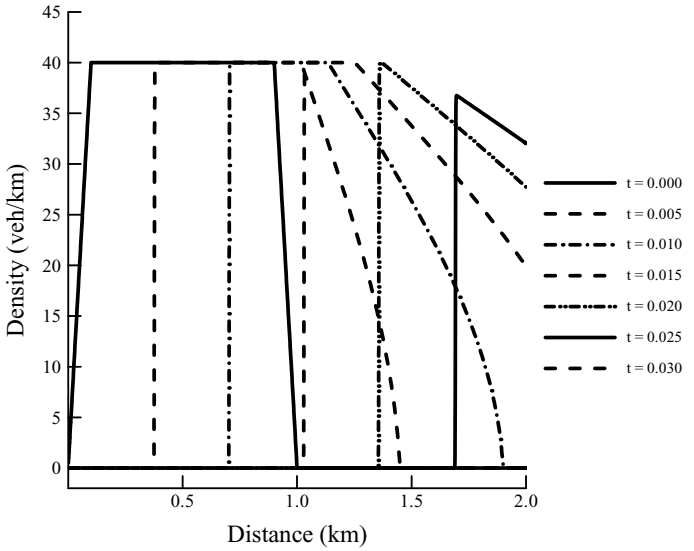

Fig. 7. Total density as a function of spatial location, for $t = 0, 0.005, 0.010, \ldots, 0.030$ h, for the case of nine-class model with identical free speed.

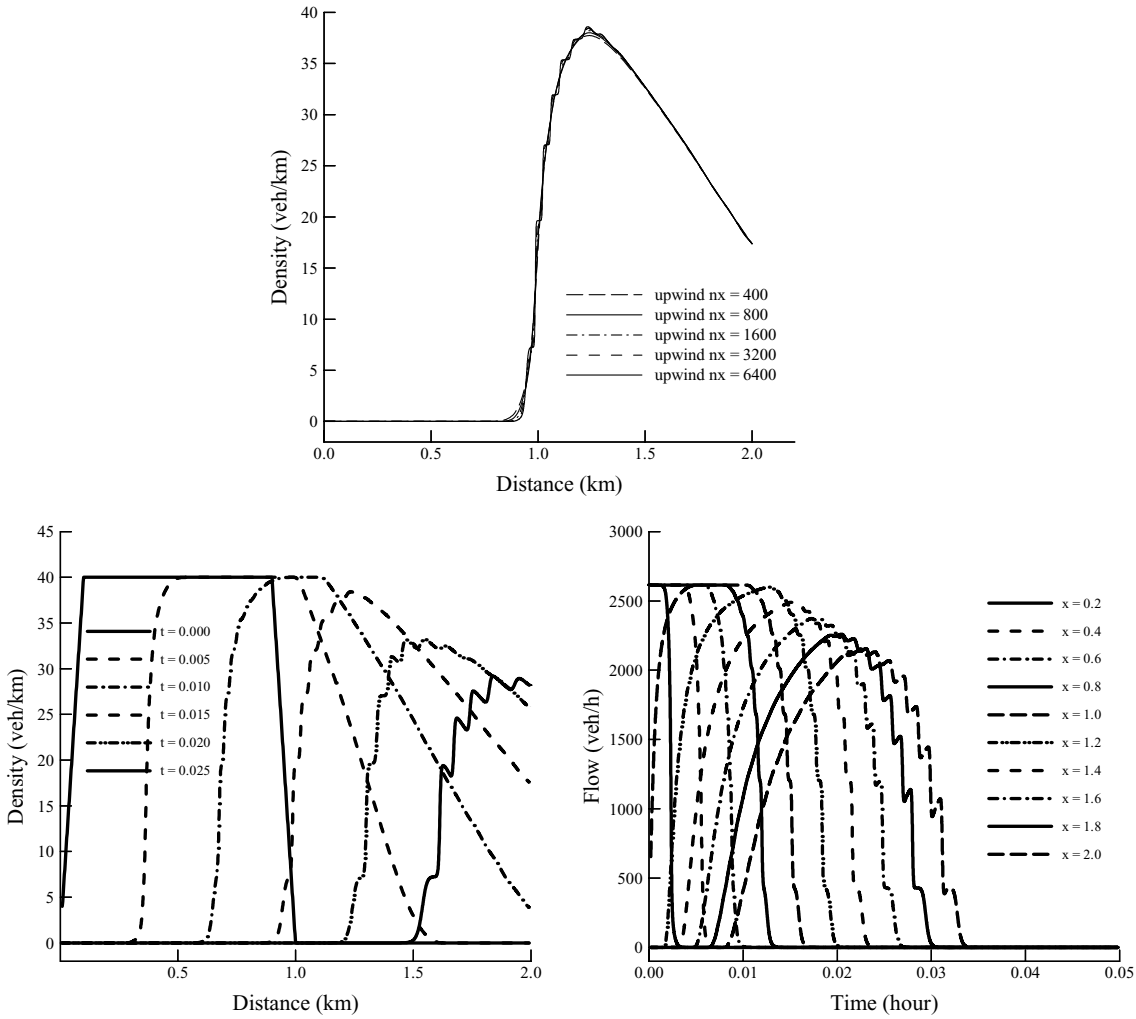

Fig. 8. First-order Godunov solver. Top: convergence with mesh refinements; bottom: density and flow evolution.

first-order Godunov scheme converges to the same solution as the other two schemes, when we overlay the solutions (not shown here).

The first-order Godunov scheme has merit in that it is computationally fast. However, the clocked times (shown in Table 1) for both the fifth-order WENO code and the first-order upwind code (Godunov in the special case of all positive eigenvalues), which achieve the same resolution, still favor the WENO scheme. Clearly the advantage of the simple and fast computation of the first-order Godunov scheme is offset by the use of more grid points to achieve higher accuracy. Although the per grid point cost of the WENO scheme is much higher than that of the first-order Godunov scheme, it is possible to code WENO to minimize the cost. This, in combination of the drastic reduction of space–time grids when using the WENO scheme rather than the Gudunov scheme, renders the total computational cost comparison for a fixed resolution to favor the WENO scheme as shown in Table 1. We also point out again that the Godunov scheme for this problem is very difficult, if not impossible, to obtain when the eigenvalues change sign.

Table 1
CPU times for the first-order Godunov scheme and the fifth-order WENO scheme at the same level of accuracy for the nine-class model in Section 4.2 (on a SunBlade 1000 workstation)

	First-order Godunov (s)	Fifth-order WENO (s)
	$nx = 1600$	$nx = 200$
$t = 0.1$ h	20	4
$t = 0.2$ h	39	8
	$nx = 6400$	$nx = 800$
$t = 0.1$ h	376	71
$t = 0.2$ h	722	138

4.3. Numerical experiments for different congestion regimes and traffic stream models

In this section, we perform more numerical experiments, using the WENO scheme with 1600 grid points (which gives numerically convergent solutions for all example calculations presented here), with different model characteristics for the MCLWR model. We still use the nine-class model with the density distribution given by Fig. 4, but we consider the following four cases:

1. The initial density distribution represents a platoon in the non-congested regime, as given in Fig. 1. The traffic stream model takes the modified Drake's form (35). This case has already been considered in the previous section.
2. The initial density distribution represents a platoon in the congested regime, as given in Fig. 9, which has a higher maximum initial density value of 120 veh/km. The traffic stream model is identical to that in Case 1.
3. The initial density distribution represents a platoon in the non-congested regime, as given in Fig. 1. The traffic stream model takes the modified Greenshields' form (36) with a jam density of $k_{\text{jam}} = 200$ veh/km,

$$u_m = U_m(k) = u_{fm}\left(1 - k/k_{\text{jam}}\right), \quad m = 1, 2, \ldots, M. \tag{36}$$

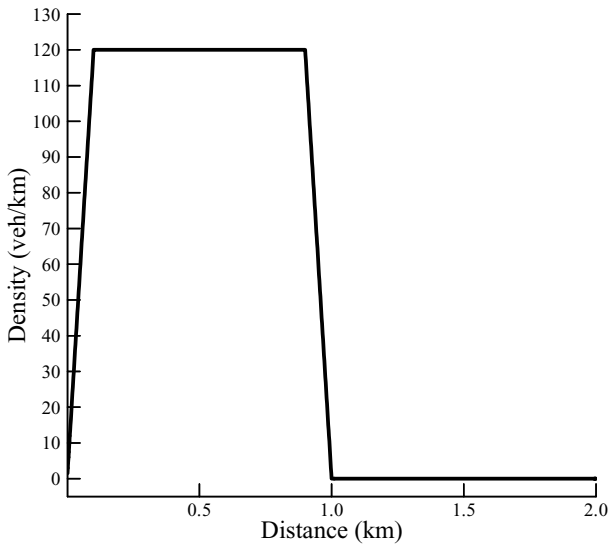

Fig. 9. Initial platoon with density at the high density regime.

4. The initial density distribution represents a platoon in the congested regime, as given in Fig. 9. The traffic stream model is identical to that in Case 3.

The density versus distance plots for various times, and the flow versus time plots for various spatial locations, are given in Figs. 6, 10, 11 and 12, respectively, for these cases. It is clear from these figures that dispersion at the tail of the platoon is limited until its density value has dropped to near or below certain critical values. These values are the optimal densities given by the Drake's and Greenshields' traffic stream

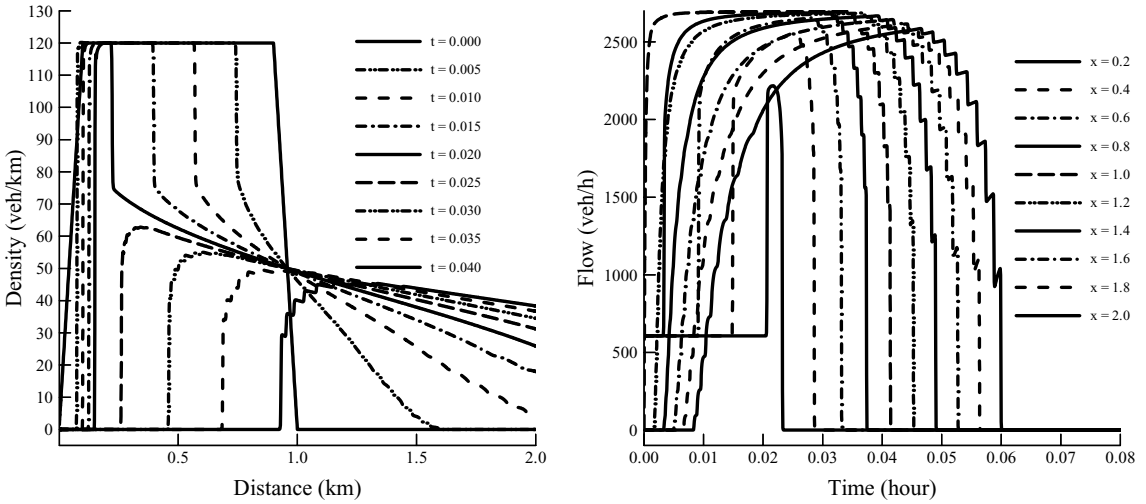

Fig. 10. Case 2. Left: total density as a function of spatial location, for $t = 0, 0.005, 0.010, \ldots, 0.025$ h; Right: the flow as a function of time t at $x = 0.2, 0.4, 0.6, \ldots, 2.0$ km.

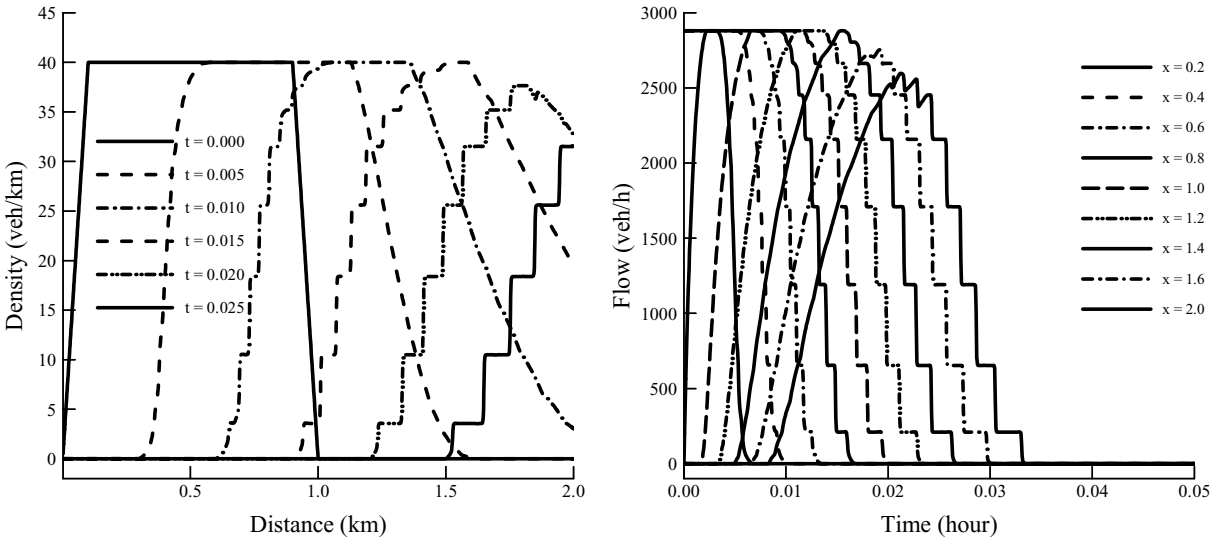

Fig. 11. Case 3. Left: total density as a function of spatial location, for $t = 0, 0.005, 0.010, \ldots, 0.025$ h; Right: the flow as a function of time t at $x = 0.2, 0.4, 0.6, \ldots, 2.0$ km.

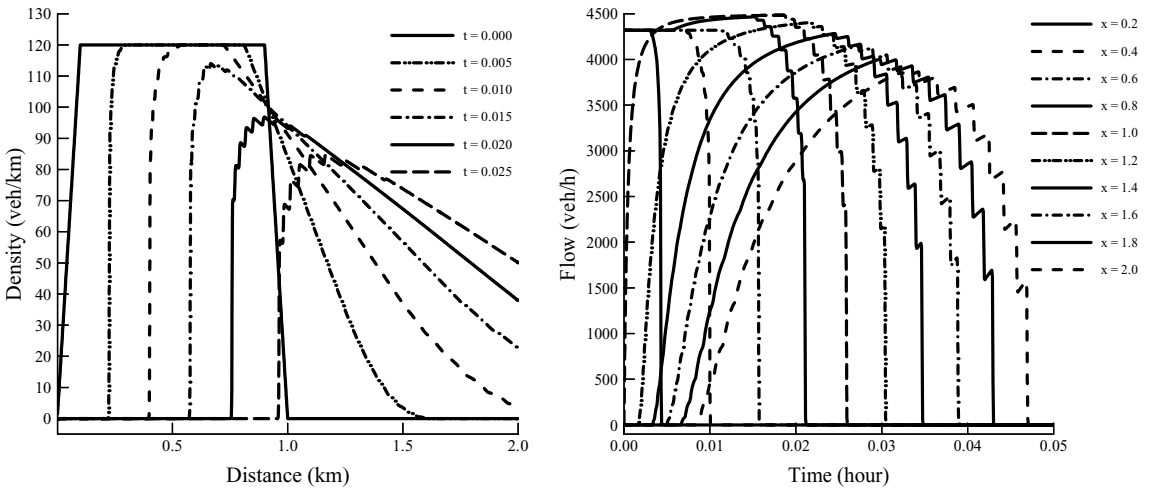

Fig. 12. Case 4. Left: total density as a function of spatial location, for $t = 0, 0.005, 0.010, \ldots, 0.025$ h; Right: the flow as a function of time t at $x = 0.2, 0.4, 0.6, \ldots, 2.0$ km.

models used. They are related to the capacity or maximum flow of the highway being analyzed. A given highway is described as operating at a congested or non-congested state when the density of the traffic stream is above or below the optimal density of the highway, respectively.

We first look at Fig. 6 for the modified Drake's model. The optimal density, k_0, is set to be 50 veh/km for this model. Initially the density of the platoon is below the optimal density and therefore the highway is not congested. As a result vehicles in the nine different classes are free to overtake and move as desired, and the platoon disperses as depicted in the figure. The second case for Drake's model is an initial platoon of density 120 veh/km, much greater than the highway's optimal density. This time the highway is operating in a congested state and this results in a non-dispersed tail of the platoon because overtaking is limited in such a congested state. The front of the platoon still can disperse because the downstream end is empty. Vehicles at the tail of the platoon however have to wait until the density drops near to or below the optimal density. They are then free to disperse again when the highway is operating in a non-congested state.

Figs. 11 and 12 represent similar cases to Figs. 6 and 10, but with the modified Drake's model replaced by the modified Greenshields' model. The optimal density of the modified Greenshields' model is given by $k_0 = k_{\text{jam}}/2$. Since k_{jam} is set to be 200 veh/km the optimal density is therefore equal to 100 veh/km. Similar results are obtained with the modified Greenshields' model. When the initial platoon has a density less than the optimal density, dispersion occurs throughout the analysis (Fig. 11). If the platoon is initially congested with a density value above the optimal, dispersion is limited (Fig. 12). Only when the density of the platoon drops back to near or below the optimal density can vehicles overtake easily and the dispersion behavior becomes clear.

4.4. Infinite number of driver classes

We might wonder what physical meaning the small staircases carry in the nine-class model. By computing with different number of classes we have observed that the number of staircases is always equal to the number of classes (this corresponds to the different wave speeds of the different combinations of classes), and the strength of those staircases decreases with the number of classes.

We could thus consider an asymptotic case when the number of classes goes to infinity. The model (3) then becomes again a scalar equation but with one more independent variable v, corresponding to the distribution of driver classes. It reads

$$\frac{\partial k(x,t,v)}{\partial t}+\frac{\partial q(x,t,v)}{\partial x}=0, \quad v\in[v_{\min},v_{\max}] \tag{37}$$

with the numerical flux given by

$$q(x,t,v)=vk(x,t,v)\exp(-(k(x,t)/k_0)^2/2) \quad \text{for modified Drake's form} \tag{38}$$

and

$$q(x,t,v)=vk(x,t,v)(1-k(x,t)/k_{\text{jam}}) \quad \text{for modified Greenshields' form.} \tag{39}$$

Other forms of traffic stream models can be considered in similar fashion. The boundary conditions are now set as a function of the class variables $v\in[v_{\min},v_{\max}]$. We remark that this continuous model has some similarity with the kinetic models, however no relaxation is involved and this can be considered as a relaxed, equilibrium model. The main difference is that, while the conventional kinetic models consider a distribution of non-equilibrium speed around an equilibrium value, our model assumes a continuous distribution of equilibrium speed.

As example calculations, we assume a modified Drake's form of traffic stream model, as in Eq. (38), with $k_0=50$ veh/km, and an initial platoon of maximum density 40 veh/km as shown in Fig. 1. The distribution of k everywhere in the platoon, as a function of v, follows a continuous curve in the shape of Fig. 13, left, which, when discretized using nine points in v, and suitably scaled, gives the original Fig. 4. Thus, the M-class model can be considered as a discretization of the continuous model (37) in the v variable. To demonstrate that the solutions from the M-class model converge to those of the continuous model (37), we plot the nine-class, 21-class and 41-class density versus distance graphs at $t=0.015$ h, in Fig. 13, right, using WENO with 1600 points, which gives numerically convergent solutions. We can clearly see that the

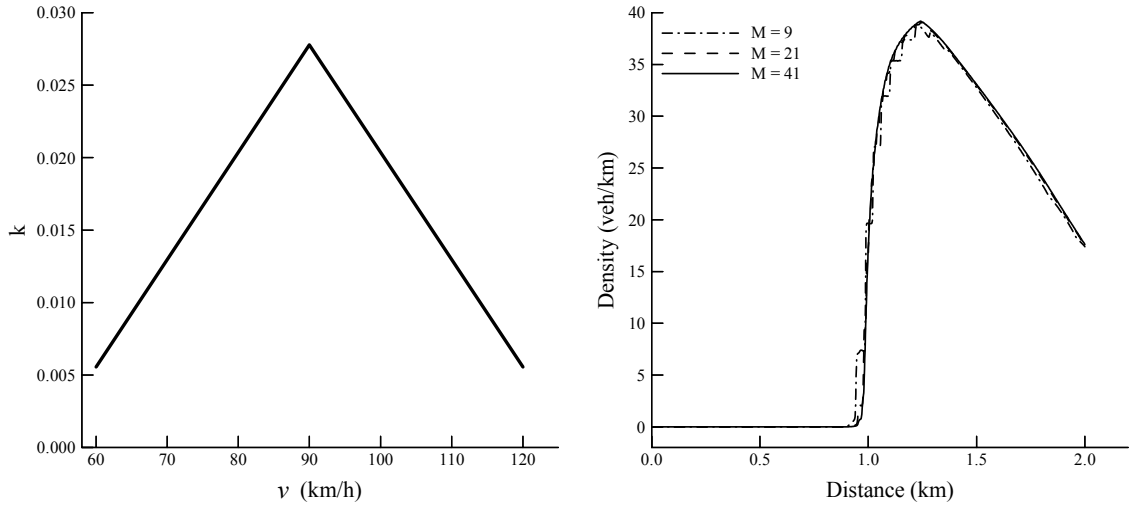

Fig. 13. Continuous in v model. Left: total density k as a function of v; Right: Convergence when the number of classes increases. Density as a function of distance at $t=0.015$. $M=9$ classes (dash-dotted line), $M=21$ class (dashed line) and $M=41$ classes (solid line).

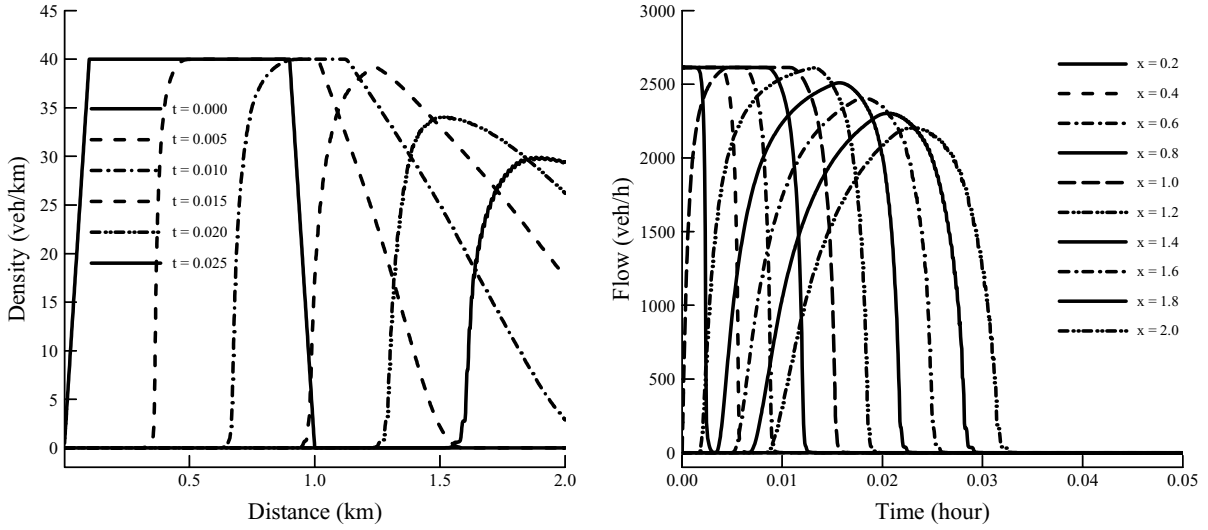

Fig. 14. Continuous in v model for $M = 41$ classes. Left: total density as a function of spatial location, for $t = 0, 0.005, 0.010, \ldots, 0.025$ h; Right: the flow as a function of time t at $x = 0.2, 0.4, 0.6, \ldots, 2.0$ km.

solutions converge to smooth curves without staircases when the number M of classes increases. There is not much noticeable difference when M increases beyond 41. In Fig. 14, we plot the density versus distance for various times on the left, and the flow versus time for various spatial locations on the right, for the continuous model (37) demonstrated by the $M = 41$ class model. It is interesting to note that a nice platoon dispersion behavior is observed for this continuous model.

5. Discussions and conclusions

The study of traffic flow using a macroscopic approach often involves a single conservation law, or a system of conservation laws that are, in general, of hyperbolic type. The scalar LWR model and those higher-order continuum models proposed so far contain hyperbolic partial differential equations. Care must be taken in solving these PDEs using numerical methods due to the existence of singularities and multiple solutions. Fortunately much work on numerical methods for hyperbolic PDEs has been carried out in the field of Computational Fluid Mechanics (CFD), which can also be applied to traffic flow problems. In this paper, we applied one of the state-of-the-art methods called weighted essentially non-oscillatory (WENO) scheme to obtain solutions for a recently proposed MCLWR model in [30]. The results of a series of numerical tests are encouraging and interesting. Several conclusions can be drawn. First, for the two-class model, the derived linearized wave speeds give reasonable predictions of the actual nonlinear wave speeds. Analysis using linearization on the MCLWR model also demonstrated that for this two-class case the class-characterized waves never travel faster than the fastest vehicle in the traffic stream.

Second, the fifth-order WENO scheme has been implemented to solve the MCLWR model and it is more efficient than the first-order Lax–Friedrichs scheme and the first-order Godunov scheme. The high-order WENO needs fewer grid points than the first-order methods to obtain solutions of the same accuracy. The reduction factor is around 64 for the Lax–Friedrichs scheme and 8 for the Godunov scheme. We remark that the WENO scheme that is studied in this paper is just a representative of high order, high resolution

schemes. Other high order, high resolution schemes may also work well on this traffic model, but we do not study them in this paper.

Third, from the convergence study of the numerical methods used in this paper, for first-order schemes, it might be premature to accept that a solution is converged, unless a very refined mesh (e.g., 25,600 points for the Lax–Friedrichs scheme) is used. Convergent solutions of the evolution of initial platoons of vehicles show that the MCLWR model produces dispersed platoons with staircase-like steps. We found that the number of steps is equal to the number of classes in the traffic stream. Linearized analysis of the two-class model in Section 2 shows that there exist two class-characterized waves, which can also be generalized to the M-class model that there would be M different class-characterized waves traveling in the traffic stream. The speed of each wave is characterized by the class-specific parameters in the MCLWR model. It is believed that the formation of staircase is caused by these class-characterized waves in the traffic stream. For the two-class test case, each staircase is composed of one class of driver only. However, this exclusivity property does not generally apply for the cases with greater number of classes.

Finally, we have extended the MCLWR model to include a continuous equilibrium speed distribution. Thus the M-class model can be considered as a discretization of this continuous model. It has been shown, by increasing M, that the continuous model can predict platoon dispersion behavior without the staircases observed in the discrete M-class model. This is quite realistic as the actual equilibrium speed distribution might be expected to be continuous in general. The actual distribution function has yet to be determined from field data; however the underlying philosophy of the MCLWR model will not change.

Acknowledgements

This collaborative research was jointly supported by the following research grants: NNSFC Grant 10028103 from the People's Republic of China (while the second author was in residence at the Department of Mathematics, University of Science and Technology of China, Hefei, Anhui 230026), ARO Grant DAAD19-00-1-0405 and NSF Grant DMS-9804985 from the USA, an Outstanding Young Researcher Award 2000 from the University of Hong Kong, and RGC Grant HKU7031/02E from the Hong Kong Research Grants Council.

References

[1] P. Bagnerini, M. Rascle, A multi-class homogenized hyperbolic model of traffic flow, SIAM Journal on Mathematical Analysis (to appear).
[2] D. Balsara, C.-W. Shu, Monotonicity preserving weighted essentially non-oscillatory schemes with increasingly high order of accuracy, Journal of Computational Physics 160 (2000) 405–452.
[3] M.J. Cassidy, R.L. Bertini, Some traffic features at freeway bottlenecks, Transportation Research 33B (1999) 25–42.
[4] M.J. Cassidy, M. Mauch, An observed traffic pattern in long freeway queues, Transportation Research 35A (2001) 143–156.
[5] C.F. Daganzo, Requiem for second-order fluid approximations of traffic flow, Transportation Research 29B (1995) 277–286.
[6] C.F. Daganzo, A continuum theory of traffic dynamics for freeways with special lanes, Transportation Research 31B (1997) 83–102.
[7] C.F. Daganzo, A behavioral theory of multi-lane traffic flow, Part I: Long homogeneous freeway sections, Transportation Research 36B (2002) 131–158.
[8] C.F. Daganzo, A behavioral theory of multi-lane traffic flow, Part II: Merges and the onset of congestion, Transportation Research 36B (2002) 159–169.
[9] C.F. Daganzo, W.H. Lin, J.M. Del Castillo, A simple physical principle for the simulation of freeways with special lanes and priority vehicles, Transportation Research 31B (1997) 103–125.
[10] J.S. Drake, J.L. Schofer, A.D. May, A statistical analysis of speed density hypothesis, Highway Research Record 154 (1967) 53–87.
[11] S. Godunov, A difference scheme for numerical computation of discontinuous solution of equations of fluid dynamics, Mathematics of the USSR-Sbornik 47 (1959) 271–306.

[12] S. Gottlieb, C.-W. Shu, E. Tadmor, Strong stability preserving high order time discretization method, SIAM Review 43 (2001) 89–112.
[13] B.D. Greenshields, A study of traffic capacity, Proceedings of the Highways Research Board 14 (1934) 448–477.
[14] S.P. Hoogendoorn, P.H.L. Bovy, Multiclass macroscopic traffic flow modelling: a multilane generalisation using gas-kinetic theory, in: A. Ceder (Ed.), Proceedings of the 14th International Symposium on Transportation and Traffic Theory, Elsevier Science Ltd., Adelaide, Australia, 1999, pp. 27–50.
[15] S.P. Hoogendoorn, P.H.L. Bovy, Continuum modelling of multiclass traffic flow, Transportation Research 34B (2000) 123–146.
[16] S.P. Hoogendoorn, P.H.L. Bovy, H. Van Lint, Short-term prediction of traffic flow conditions in a multilane multiclass network, in: M.A.P. Taylor (Ed.), Proceedings of the 15th International Symposium on Transportation and Traffic Theory, Elsevier Science Ltd., Adelaide, Australia, 2002, pp. 625–651.
[17] G.S. Jiang, C.-W. Shu, Efficient implementation of weighted ENO schemes, Journal of Computational Physics 126 (1996) 202–228.
[18] J.P. Lebacque, Semimacroscopic simulation of urban traffic, Paper presented at the International 84 Minneapolis Summer Conference, ASME, 1984.
[19] J.P. Lebacque, The Godunov scheme and what it means for first order traffic flow models, in: J.B. Lesort (Ed.), Proceedings of the 13th International Symposium on Transportation and Traffic Theory, Elsevier Science Ltd., Lyon, France, 1996, pp. 647–677.
[20] R.J. LeVeque, Numerical Methods for Conservation Laws, Birkhauser, Basel, 1992.
[21] M.J. Lighthill, G.B. Whitham, On kinematic waves: II a theory of traffic flow on long crowded roads, Proceedings of the Royal Society, London, Series A 229 (1955) 317–345.
[22] M. Mauch, M.J. Cassidy, Freeway traffic oscillations: observations and predictions, in: M.A.P. Taylor (Ed.), Proceedings of the 15th International Symposium on Transportation and Traffic Theory, Elsevier Science Ltd., Adelaide, Australia, 2002, pp. 653–673.
[23] P.G. Michalopoulos, D.E. Beskos, J.K. Lin, Analysis of interrupted traffic flow by finite difference methods, Transportation Research 18B (1984) 409–421.
[24] P.I. Richards, Shock waves on the highway, Operations Research 4 (1956) 42–51.
[25] C.-W. Shu, Essentially non-oscillatory and weighted essentially non-oscillatory schemes for hyperbolic conservation laws, in: B. Cockburn, C. Johnson, C.-W. Shu, E. Tadmor, A. Quarteroni (Eds.), Advanced Numerical Approximation of Nonlinear Hyperbolic Equations, Lecture Notes in Mathematics, vol. 1697, Springer, New York, 1998, pp. 325–432.
[26] C.-W. Shu, High order finite difference and finite volume WENO schemes and discontinuous Galerkin methods for CFD, International Journal of Computational Fluid Dynamics 17 (2003) 107–118.
[27] C.-W. Shu, S. Osher, Efficient implementation of essentially non-oscillatory shock capturing schemes, Journal of Computational Physics 77 (1988) 439–471.
[28] G.B. Whitham, Linear and Nonlinear Waves, Wiley, USA, 1974.
[29] J.R. Windover, M.J. Cassidy, Some observed details of freeway traffic evolution, Transportation Research 35A (2001) 881–894.
[30] G.C.K. Wong, S.C. Wong, A multi-class traffic flow model – an extension of LWR model with heterogeneous drivers, Transportation Research 36A (2002) 827–841.
[31] S.C. Wong, G.C.K. Wong, An analytical shock-fitting algorithm for LWR kinematic wave model embedded with linear speed–density relationship, Transportation Research 36B (2002) 683–706.
[32] H.M. Zhang, W.H. Lin, Some recent developments in continuum vehicular traffic theory, in: M.A.P. Taylor (Ed.), Proceedings of the 15th International Symposium on Transportation and Traffic Theory, Elsevier Science Ltd., Adelaide, Australia, 2002, pp. 607–624.
[33] H.M. Zhang, W.H. Lin, A kinematic wave traffic flow model for mixed traffic, Transportation Research Record 1802 (2002) 197–204.